PHYSICAL REVIEW B **78**, 220101(R) (2008)

High-pressure nanocrystalline structure of a shock-compressed single crystal of iron

James A. Hawreliak,* Daniel H. Kalantar, James S. Stölken, Bruce A. Remington, and Hector E. Lorenzana
Lawrence Livermore National Laboratory, Livermore, California 94550, USA

Justin S. Wark
Department of Physics, Clarendon Laboratory, University of Oxford, Parks Road, Oxford OX1 3PU, United Kingdom
(Received 13 November 2008; published 22 December 2008)

We discuss the grain-size measurements made during shock compression using *in situ* x-ray diffraction. Our experiments have shown unambiguously that single-crystal iron shock loaded above 13 GPa along the [100] direction will transform from the ambient α phase (bcc) to a highly ordered polycrystalline ϵ phase (hcp). Here, we present a detailed shape analysis of the diffraction peaks using a modified Warren-Averbach method to quantify the microstructure of shock-compressed high-pressure iron. The ϵ phase was determined through this method to have grain sizes between 2 and 15 nm, in reasonable agreement with results from large-scale molecular-dynamics simulations. We conclude that single-crystal iron becomes nanocrystalline in shock transforming from α to ϵ phase.

DOI: 10.1103/PhysRevB.78.220101 PACS number(s): 62.50.Ef, 61.72.Hh, 61.46.Hk, 61.05.cp

The impact of the atomic arrangement on materials properties subjected to high levels of stress and temperature has been studied for nearly a century.[1] Structural changes have been shown to occur in quasistatic experiments, such as compression in a diamond-anvil cell,[2] as well as highly dynamic situations, such as shock loading.[3] While atomic arrangement is of crucial importance, it is one of the several key attributes that play central roles in determining complicated material properties, such as strength and failure.[4] With respect to these latter two properties, the microstructure of a material can significantly affect material performance, especially at high-pressure and high-strain rate conditions. A recognized phenomenon known to dramatically increase material strength with decreasing grain size is the Hall-Petch effect.[5,6] It follows that our ability to fundamentally understand and predict material behavior in extreme environments depends partially but crucially on understanding the microstructure of the high-pressure state of a solid. While literature exits describing residual defect microstructure of samples upon recovery from shock experiments,[7,8] the insight such postshock measurements afford is fundamentally limited by the dynamic release process after the pressure pulse, which can radically reduce defect densities and alter the microstructure from that which was present under peak transient compression. To date, there have been no reported *in situ* measurements of the microstructure during shock loading due to the experimental challenges associated with *in situ* measurements of microstructure. Accordingly, a measurement of grain size would constitute a critical step in developing a basic understanding of microstructure dependence on loading history and equation of state. In this Rapid Communication, we describe *in situ* measurements of microstructure for a dynamically loaded material by use of x-ray diffraction from the high-pressure phase of shock-compressed single-crystal iron. We describe a nanocrystalline material, which is highly textured that exists only in a high-pressure state, generated from single-crystal iron under dynamic conditions.

The α-ϵ phase transition in iron has been one of the most studied high-pressure transitions in material science owing to iron's fundamentally and geophysical importance. For the shock physics community it represents a major success as the α-ϵ phase transition in iron was first detected in shock loading before it was confirmed at a similar pressure under static experiments.[9,10] While the time scale of the applied pressure varies greatly between the dynamic and static experiments, it had always been assumed that the transition observed in these experiments was the same. Using *in situ* x-ray diffraction, we recently confirmed that single-crystal iron indeed transforms to the high-pressure ϵ phase[11] when shocked along the [100] direction. A detailed analysis of the ϵ-phase data provided insight into the transition mechanism and the difference in the c/a ratios observed between the transient and static experiments.[12] The transition of iron from bcc to hcp due to shock loading of a single crystal along the [100] direction consists of an elastic compression of the lattice along the [100] direction with the formation of a pseudohexagon in the [110] plane. By a shift of alternate (110) planes the hexagons in the (110) bcc planes become (0001) planes in the high-pressure hcp system. Due to the symmetry about the compression axis of the bcc lattice it is energetically degenerate for the shuffle of {110} planes to occur along any of the four [110] directions, with antiparallel pairs of [110] shuffles yielding the same orientation of hcp. An example of how this degeneracy in the transition yields a polycrystalline structure is shown in Fig. 1, where the shock direction is into the page. In this figure, we show the α phase before the transition along with two of the four possible hcp variants. Variant 1, where the shuffle happens in the $[\bar{1}10]$ direction relative to the original bcc structure, establishes the high-pressure ϵ phase with the c axis along the original [110] direction. Variant 2 occurs due to a shift along the [110] direction and the c axis along the $[1\bar{1}0]$ direction. While two of the four possible variants are shown, it is these variants, which lead to a polycrystalline structure of the high-pressure phase.

The experiments were performed using the OMEGA,[13] Janus, and Vulcan[14] lasers. Samples of 200–270 μm thick single-crystal [001] iron with a purity of 99.94% from Accumet Materials and 10 μm thin single-crystal foils from the

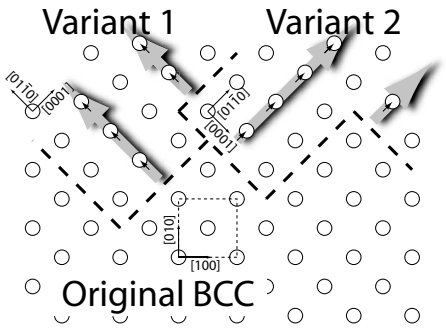

FIG. 1. A schematic view of the generation of the polycrystalline high-pressure ϵ phase in iron due to the degeneracy of the directions in which the shuffle of alternating planes can occur. In this figure, the shock direction is into the page.

University of Aarhus were coated with a 16–20 μm parylene-*N* ablator layer followed by a 0.1 μm aluminum shine-through layer. These samples were shock loaded by direct laser irradiation at 2×10^{10} to 1×10^{12} W/cm^2 using 2–6 ns constant intensity laser pulses. The diameter of the region on the crystal shocked by the laser was 2–3 mm. The resulting shock pressure covered a range of pressures that spanned the transition pressure.

The shocked iron single crystals were interrogated by wide-angle *in situ* diffraction, which has been described extensively elsewhere.[15,16] In these experiments, a source of 1.85 Å iron *K*-shell x rays was created by laser beams focused on a metal foil synchronous to the shock-driving beams. X rays were generated from a 100–200 μm diameter quasimonochromatic source and diffracted from the surface of the crystal 0.7–1.3 mm away. The diffracted x rays were recorded on time integrating film or image plate detector. Figure 2 shows a schematic of the diffraction from a single crystal in this geometry. Temporal resolution in this experiment is provided by varying the duration of the x-ray pulse, which closely follows the 2–4 ns optical laser pulse that creates them.[17] For the 200 μm thick iron samples, the x rays were diffracted only from the shocked side of the iron crystal in reflection geometry—which we refer to as Bragg geometry. For the 10 μm thin samples it was also possible to record diffracted x rays in transmission, which we refer to

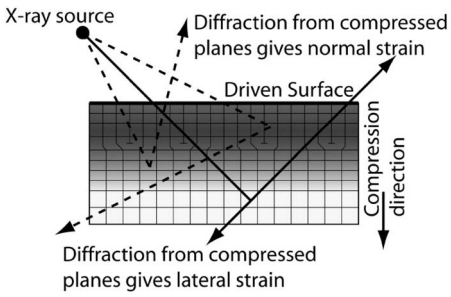

FIG. 2. A schematic of the *in situ* x-ray diffraction technique. A quasimonochromatic source is placed close to a single crystal of material so that x rays are incident at a wide range of angles. The x rays diffract from regions of the sample where the Bragg condition is met. A change in angle of the diffracted x rays indicates that a change in the lattice has occurred.

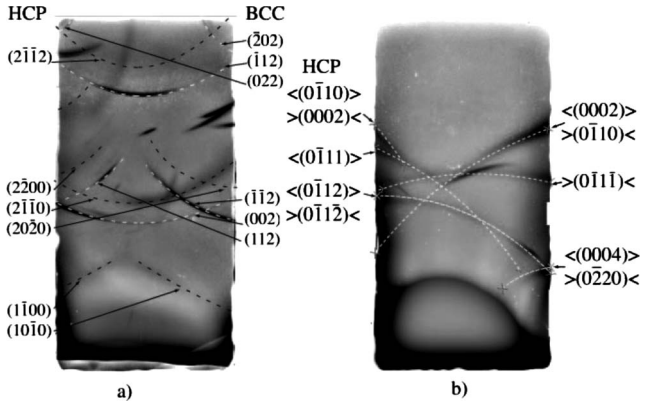

FIG. 3. X-ray diffraction data showing diffraction lines consistent with an hcp high-pressure phase in (a) Bragg (reflected) where the static bcc material is denoted with white dashed lines and the higher-pressure hcp with black dashed lines and (b) Laue (transmitted) where there is no separation upon compression of the bcc and hcp diffraction planes and only the hcp planes are labeled.

as Laue geometry. Owing to the divergence of the x rays and the large angle, which the crystal subtends to the x-ray source, x rays diffracted from many different lattice planes in the crystal are simultaneously recorded on two wide-angle multiple film packs covering a total of nearly 2π steradians around the sample.[15]

In the raw data shown in Fig. 3, the diffracted x rays appear as curves that are identified with their appropriate plane labels. The 1.85 Å x rays have a penetration depth of about 10 μm into the sample. Due to this finite penetration depth and the duration of the x-ray pulse we observe at least two lines associated with each diffraction plane—the unshocked and shock-compressed states. The diffraction lines from the unshocked part of the crystal provide a reference from which to measure the change in Bragg angle for each reflection. For shock pressures above the transition pressure, we observe up to two further curves, the first corresponding to elastic compression of the bcc lattice and the second to a broader feature, which is consistent with the period doubling of the bcc structure to hcp. At the highest pressures, however, the crystals are overdriven and the elastic signature is not observed, as in Fig. 3. The diffraction lines from the unshocked lattice are significantly narrower than the shocked diffraction lines, proving that the broadening is not due to the instrument function or the initial state of the crystal. Transmitted x-ray diffraction has shown that the material is polycrystalline in nature by the generation of diffraction lines consistent with different orientations of hcp.[11,12] We now consider the broadening of the diffraction lines in iron, which can originate from two sources: first the finite grain size of the hcp phase or second a strain gradient distribution within the high-pressure phase.

The diffuse and continuous nature of the diffraction curves, as seen in Fig. 3, sets an upper bound on the possible grain size. In control experiments with the same experimental setup and characterized large-grain samples diffraction from individual grains appeared as discrete dashes.[18] Based on this calibration we estimate that we would have observed discrete dashes in our diffraction signal if the grains had been

larger than 5 μm in the high-pressure phase.

To obtain a more refined handle on the grain size we use a modified Warren-Averbach analysis[19] to fit the shape of the diffraction peak of the high-pressure iron ϵ phase. This technique, originally put forward by Warren and Averbach in 1950,[19] uses a Fourier transform of the profile of a collection of diffraction peaks to extract the grain-size distribution and strain information used to determine material microstructure. The Fourier transform of the profile of a single diffraction peak is described by the function $A_n(l)$, where n is the transformed variable and l is the length of the scattering vector (i.e., the diffraction plane). This function consists of two components, $A_n(l)=A_n^S A_n^D(l)$. One component, A_n^S, is determined by the size distribution of grains in the sample, which has no dependence on the scattering vector, l, and the second, $A_n^D(l)$, is due to nonuniform strain caused by defects and large-scale gross strain gradients, which depend on the scattering vector. Each term is dependent on the distribution of grain sizes and strains as described by

$$A_n^S = \frac{1}{N_3}\int_{i=n}^{\infty}(i-n)p(i)di, \tag{1}$$

$$A_n^D(l) = \langle \cos(2\pi l Z_n)\rangle, \tag{2}$$

where $p(i)$ is the probability that a grain has a size i, $p(Z_n)$ is the probability of a strain Z between planes separated by n atomic layers, and the distortion term $A_n^D(l)$ assumes that the strain distribution is symmetric (the antisymmetric part has been ignored for simplicity). In static experiments it is possible to resolve the peak shapes over 2 orders of magnitude in intensity, yielding high-fidelity measurements of many components of the peak transform.[20,21] In the dynamic experiments described here, the background x-ray signal due to broadband emission from the backlighter and emission from the plasma generated by the drive laser limits the signal to noise to a fraction of what is possible in static experiments. To accommodate this we simplify the analysis by assuming a single grain size and a Gaussian distribution of strain. Then the broadening of the peak is described by[22]

$$A_n^S = \exp\left(-\pi\frac{n^2}{\sigma^2}\right), \tag{3}$$

where σ is the grain size and the strain distribution is described by a single function $p(\epsilon)$, where $\epsilon=Z_n/n$ is the normalized strain and the broadening is

$$A_n^D(l) = \exp(2\pi^2 l^2 n^2 \langle \epsilon^2\rangle). \tag{4}$$

Using these two approximations, a diffraction peak is described by a Gaussian distribution,

$$a(g) = \exp\left(-\frac{g^2}{W^2}\right), \quad W^2 = B^2 + A^2 l^2, \tag{5}$$

and g is the scattering vector associated with the diffraction plane l. By plotting W^2 versus l^2 for a series of peaks, a linear fit results in an estimate of the grain size from the intercept, $B=a_0/\sqrt{\pi}\sigma$, where a_0 is the unit-cell size and of the rms strain from the slope $A=2\sqrt{2}\pi\sqrt{\langle\epsilon^2\rangle}$.

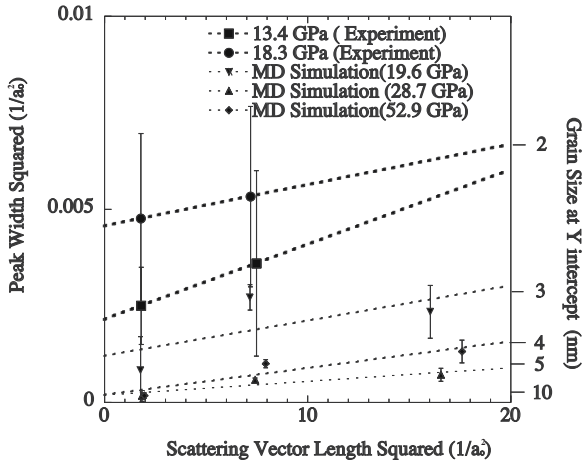

FIG. 4. A plot of the square of the peak widths (in units inverse cell size, a_0) as a function of the square to the scattering vector length (the modified Warren-Averbach analysis). The gradual slopes of the lines suggest the broadening is dominated by the grain size of the high-pressure phase. The right axis label identifies the grain size associated with the peak width, where the y intercept gives the grain size.

In Fig. 4, we plot some example data of peak width versus scattering vector. We applied the modified Warren-Averbach analysis to the (1100) and (2200) planes of the high-pressure phase, which correspond to the original (112) plane and period doubling of the (112) plane (which is forbidden for bcc). We record two orders of the same diffraction plane because the uniaxial nature of the compression could lead to a grain size or strain structure that is highly directionally dependent. Due to the single-crystal nature of the sample, diffraction planes with the same directional vectors need to be used to provide a solution for grain size and strain. The plotted widths represent a series of best fitted line outs from the data. While the errors inferred from the experimental data plotted in Fig. 4 appear large, the grain size can still be constrained to an order of 2–15 nm, with very low residual strain broadening ($\approx 0.2\% \pm 0.8\%$). Also plotted in Fig. 4 is a similar analysis applied to simulated x-ray diffraction from large-scale molecular-dynamics (MD) simulations with a grain size as low as 4 nm for 19.6 GPa shock and as large as 10 nm for the 28.7 and 52.9 GPa shocks.[23] The deviation of the MD simulations from a linear fit suggests the strain does not follow a Gaussian distribution in the MD simulation. While the determination of a strain profile cannot be made in the experiment, the gradual slope of peak width suggests that the dominant mechanism for broadening of the diffraction lines is grain size, both in the experiment and MD simulations.

This analysis represents a measurement of grain size of a material, which has undergone a phase transition during dynamic compression using *in situ* x-ray diffraction. By measuring multiple orders of a diffraction plane simultaneously while the material is under compression, we were able to used a simplified Warren-Averbach analysis to fit the peak broadening of the (1100) and (2200) planes and extract a grain size on the order of 2–15 nm with very little residual strain (0.2%). This result is consistent with large-scale MD simulations of the α-ϵ phase transition in iron. Energetically

such a highly ordered polycrystalline end state would be expected since four degenerate transition pathways exist for iron compressed along the bcc [100] axis.

Single-crystal iron shock compressed along the [100] direction offers a case of a well-ordered phase transition. In this case the elastic response of the atoms before the transition facilitates a compression-shuffle mechanism for the transition, leading to a subnanosecond transition to a polycrystalline structure with grains of four orientations. These two orientations with well-aligned diffraction planes allow recordable diffraction with a single-crystal diagnostic. If the compression were more hydrostatic in nature as suggested by static experiments a different transition mechanism[24] would lead to a more complex final hcp arrangement that may not have been diagnosed with our experimental setup. Large-scale MD simulations suggest shock compression along different crystallographic axes (110 and 111) in single-crystal iron may lead to a mixed high-pressure stage of hcp and fcc with smaller grains,[25] which would require polycrystalline diffraction to determine the high-pressure structure.[26]

Signal-to-noise levels resulting from these laser-based techniques limit the microstructural information that can be extracted on a single shot. With next generation x-ray free electron laser sources becoming available by 2009, there is the potential to increase the x-ray intensity by a factor of 10^6 (10^3 more photons in 10^3 shorter time scale).[27] This increase in x-ray signal will yield peak shapes, which cover similar intensity scales as those in static experiments, potentially allowing a more detailed analysis of the microstructure using a fuller version of the Warren-Averbach technique.

The authors thank the staff at the Vulcan Laser Facility at the Rutherford Appleton Laboratory, the staff at Janus laser at Lawrence Livermore National Laboratory, and the staff and University of Rochester Laboratory for Laser Energetics. This work was performed under the auspices of the U.S. Department of Energy by Lawrence Livermore National Laboratory under Contract No. DE-AC52-07NA27344 supported by the LDRD program under Project No. 06-SI-004 at LLNL. Additional support was provided by the DOE under Grants No. DEFG0398DP00212 and No. DEFG0300SF2202 and by the U.K. EPSRC under Grant No. GR/R25699/01.

*hawreliak1@llnl.gov

[1] P. W. Bridgman, *Collected Experimental Papers* (Harvard University Press, Cambridge, 1964).
[2] H. Mao, W. A. Bassett, and T. Takahashi, J. Appl. Phys. **38**, 272 (1967).
[3] J. C. Boettger and D. C. Wallace, Phys. Rev. B **55**, 2840 (1997).
[4] D. L. Preston, D. L. Tonks, and D. C. Wallace, J. Appl. Phys. **93**, 211 (2003).
[5] E. O. Hall, Nature (London) **173**, 948 (1954).
[6] A. H. Chokshi, A. Rosen, J. Karch, and H. Gleiter, Scr. Metall. **23**, 1679 (1989).
[7] M. A. Meyers, F. Gregori, B. K. Kad, M. S. Schneider, D. H. Kalantar, B. A. Remington, G. Ravichandran, T. Boehly, and J. S. Wark, Acta Mater. **51**, 1211 (2003).
[8] M. S. Schneider, B. K. Kad, F. Gregori, D. Kalantar, B. A. Remington, and M. A. Meyers, Metall. Mater. Trans. A **35**, 2633 (2004).
[9] D. Bancroft, E. L. Peterson, and S. Minshall, J. Appl. Phys. **27**, 291 (1956).
[10] J. Jamieson and A. W. Lawson, J. Appl. Phys. **33**, 776 (1962).
[11] D. H. Kalantar *et al.*, Phys. Rev. Lett. **95**, 075502 (2005).
[12] J. Hawreliak *et al.*, Phys. Rev. B **74**, 184107 (2006).
[13] T. R. Boehly *et al.*, in *Proceedings of the Tenth Topical Conference on High Temperature Plasma Diagnostics* (AIP, Rochester, NY, 1995), Vol. 66, p. 508.
[14] C. N. Danson, L. J. Barzanti, Z. Chang, A. E. Damerell, C. B. Edwards, S. Hancock, M. H. R. Hutchinson, M. H. Key, S. Luan, and R. R. Mahadeo, Opt. Commun. **103**, 392 (1993).
[15] D. Kalantar *et al.*, Rev. Sci. Instrum. **74**, 1929 (2003).
[16] D. H. Kalantar *et al.*, Rev. Sci. Instrum. **70**, 629 (1999).
[17] D. W. Phillion and C. J. Hailey, Phys. Rev. A **34**, 4886 (1986).
[18] D. H. Kalantar *et al.*, Phys. Plasmas **10**, 1569 (2003).
[19] B. E. Warren and B. L. Averbach, J. Appl. Phys. **21**, 595 (1950).
[20] T. Ungar and A. Borbely, Appl. Phys. Lett. **69**, 3173 (1996).
[21] T. Ungar, S. Ott, P. G. Sanders, A. Borbely, and J. R. Weertman, Acta Mater. **46**, 3693 (1998).
[22] B. E. Warren, *X-ray Diffraction* (Dover, New York, 1990).
[23] K. Kadau, T. C. Germann, P. S. Lomdahl, and B. L. Holian, Science **296**, 1681 (2002).
[24] F. M. Wang and R. Ingalls, Phys. Rev. B **57**, 5647 (1998).
[25] K. Kadau, T. C. Germann, P. S. Lomdahl, and B. L. Holian, Phys. Rev. B **72**, 064120 (2005).
[26] J. Hawreliak, H. E. Lorenzana, B. A. Remington, S. Lukezic, and J. S. Wark, Rev. Sci. Instrum. **78**, 083908 (2007).
[27] J. Arthur, G. Materlik, R. Tatchyn, and H. Winick, in *Proceedings of the Fifth International Conference on Synchrotron Radiation Instrumentation* (AIP, Stony Brook, NY, 1995), Vol. 66, pp. 1987–1989.